CUORE and beyond: bolometric techniques to explore inverted neutrino mass hierarchy

D. R. Artusa[a,b], F. T. Avignone III[a], O. Azzolini[c], M. Balata[b], T. I. Banks[d,e,b], G. Bari[f], J. Beeman[g], F. Bellini[h,i],
A. Bersani[j], M. Biassoni[k,l], C. Brofferio[k,l], C. Bucci[b], X. Z. Cai[m], A. Camacho[c], L. Canonica[b], X. G. Cao[m],
S. Capelli[k,l], L. Carbone[l], L. Cardani[h,i], M. Carrettoni[k,l], N. Casali[b], D. Chiesa[k,l], N. Chott[a], M. Clemenza[k,l],
S. Copello[n], C. Cosmelli[h,i], O. Cremonesi[l,*], R. J. Creswick[a], I. Dafinei[i], A. Dally[o], V. Datskov[l], A. De Biasi[c],
M. M. Deninno[f], S. Di Domizio[n,j], M. L. di Vacri[b], L. Ejzak[o], D. Q. Fang[m], H. A. Farach[a], M. Faverzani[k,l],
G. Fernandes[n,j], E. Ferri[k,l], F. Ferroni[h,i], E. Fiorini[l,k], M. A. Franceschi[p], S. J. Freedman[e,d,1], B. K. Fujikawa[e],
A. Giachero[k,l], L. Gironi[k,l], A. Giuliani[q], J. Goett[b], P. Gorla[b], C. Gotti[k,l], T. D. Gutierrez[r], E. E. Haller[g,s], K. Han[e],
K. M. Heeger[t], R. Hennings-Yeomans[d], H. Z. Huang[u], R. Kadel[v], K. Kazkaz[w], G. Keppel[c], Yu. G. Kolomensky[d,v],
Y. L. Li[m], C. Ligi[p], X. Liu[u], Y. G. Ma[m], C. Maiano[k,l], M. Maino[k,l], M. Martinez[x], R. H. Maruyama[t], Y. Mei[e],
N. Moggi[f], S. Morganti[i], T. Napolitano[p], S. Nisi[b], C. Nones[y], E. B. Norman[w,z], A. Nucciotti[k,l], T. O'Donnell[d], F. Orio[i],
D. Orlandi[b], J. L. Ouellet[d,e], M. Pallavicini[n,j], V. Palmieri[c], L. Pattavina[b], M. Pavan[k,l], M. Pedretti[w], G. Pessina[l],
V. Pettinacci[i], G. Piperno[h,i], C. Pira[c], S. Pirro[b], E. Previtali[l], V. Rampazzo[c], C. Rosenfeld[a], C. Rusconi[l], E. Sala[k,l],
S. Sangiorgio[w], N. D. Scielzo[w], M. Sisti[k,l], A. R. Smith[aa], L. Taffarello[ab], M. Tenconi[q], F. Terranova[k,l], W. D. Tian[m],
C. Tomei[i], S. Trentalange[u], G. Ventura[ac,ad], M. Vignati[i], B. S. Wang[w,z], H. W. Wang[m], L. Wielgus[o], J. Wilson[a],
L. A. Winslow[u], T. Wise[t,o], A. Woodcraft[ae], L. Zanotti[k,l], C. Zarra[b], B. X. Zhu[u], S. Zucchelli[af,f]

[a]*Department of Physics and Astronomy, University of South Carolina, Columbia, SC 29208 - USA*
[b]*INFN - Laboratori Nazionali del Gran Sasso, Assergi (L'Aquila) I-67010 - Italy*
[c]*INFN - Laboratori Nazionali di Legnaro, Legnaro (Padova) I-35020 - Italy*
[d]*Department of Physics, University of California, Berkeley, CA 94720 - USA*
[e]*Nuclear Science Division, Lawrence Berkeley National Laboratory, Berkeley, CA 94720 - USA*
[f]*INFN - Sezione di Bologna, Bologna I-40127 - Italy*
[g]*Materials Science Division, Lawrence Berkeley National Laboratory, Berkeley, CA 94720 - USA*
[h]*Dipartimento di Fisica, Sapienza Università di Roma, Roma I-00185 - Italy*
[i]*INFN - Sezione di Roma, Roma I-00185 - Italy*
[j]*INFN - Sezione di Genova, Genova I-16146 - Italy*
[k]*Dipartimento di Fisica, Università di Milano-Bicocca, Milano I-20126 - Italy*
[l]*INFN - Sezione di Milano Bicocca, Milano I-20126 - Italy*
[m]*Shanghai Institute of Applied Physics, Chinese Academy of Sciences, Shanghai 201800 - China*
[n]*Dipartimento di Fisica, Università di Genova, Genova I-16146 - Italy*
[o]*Department of Physics, University of Wisconsin, Madison, WI 53706 - USA*
[p]*INFN - Laboratori Nazionali di Frascati, Frascati (Roma) I-00044 - Italy*
[q]*Centre de Spectrométrie Nucléaire et de Spectrométrie de Masse, 91405 Orsay Campus - France*
[r]*Physics Department, California Polytechnic State University, San Luis Obispo, CA 93407 - USA*
[s]*Department of Materials Science and Engineering, University of California, Berkeley, CA 94720 - USA*
[t]*Department of Physics, Yale University, New Haven, CT 06520 - USA*
[u]*Department of Physics and Astronomy, University of California, Los Angeles, CA 90095 - USA*
[v]*Physics Division, Lawrence Berkeley National Laboratory, Berkeley, CA 94720 - USA*
[w]*Lawrence Livermore National Laboratory, Livermore, CA 94550 - USA*
[x]*Laboratorio de Fisica Nuclear y Astroparticulas, Universidad de Zaragoza, Zaragoza 50009 - Spain*
[y]*Service de Physique des Particules, CEA / Saclay, 91191 Gif-sur-Yvette - France*
[z]*Department of Nuclear Engineering, University of California, Berkeley, CA 94720 - USA*
[aa]*EH&S Division, Lawrence Berkeley National Laboratory, Berkeley, CA 94720 - USA*
[ab]*INFN - Sezione di Padova, Padova I-35131 - Italy*
[ac]*Dipartimento di Fisica, Università di Firenze, Firenze I-50125 - Italy*
[ad]*INFN - Sezione di Firenze, Firenze I-50125 - Italy*
[ae]*SUPA, Institute for Astronomy, University of Edinburgh, Blackford Hill, Edinburgh EH9 3HJ - UK*
[af]*Dipartimento di Fisica, Università di Bologna, Bologna I-40127 - Italy*

Abstract

The CUORE (Cryogenic Underground Observatory for Rare Events) experiment will search for neutrinoless double beta decay of ^{130}Te. With 741 kg of TeO$_2$ crystals and an excellent energy resolution of 5 keV (0.2%) at the region of interest, CUORE will be one of the most competitive neutrinoless double beta decay experiments on the horizon. With five years of live time, CUORE projected neutrinoless double beta decay half-life sensitivity is 1.6×10^{26} y at 1σ (9.5×10^{25} y at the 90% confidence level), which corresponds to an upper limit on the effective Majorana mass in the range 40–100 meV (50–130 meV). Further background rejection with auxiliary light detector can significantly improve the search sensitivity and competitiveness of bolometric detectors to fully explore the inverted neutrino mass hierarchy with ^{130}Te and possibly other double beta decay candidate nuclei.

1. Neutrinoless double beta decay

The nature of massive neutrinos, i.e, whether neutrinos are their own anti-particles, is of fundamental importance to understand the origin of neutrino mass, and in a broader sense, to explore the symmetries of lepton sector (c.f. [1]). Neutrinoless double beta decay ($0\nu\beta\beta$) is the only practical probe to the nature of neutrino (c.f. [2, 3]).

Within the Standard Model, double beta decay with two daughter neutrinos ($2\nu\beta\beta$) $(Z, A) \rightarrow (Z + 2, A) + 2e^- + 2\bar{\nu}_e$ is an allowed 2nd-order weak process and observed in a dozen or so isotopes where the single beta decay is energetically forbidden or kinematically suppressed. If neutrinos are their own antiparticles (called Majorana particles), the $\bar{\nu}_e$ from one single beta decay may undergo helicity flipping and get absorbed in the second beta decay vertex as a ν_e, which results no neutrino emission and lepton number violation (LNV): $(Z, A) \rightarrow (Z + 2, A) + 2e^-$. In fact, $0\nu\beta\beta$ is by far the most realistic mechanism of all the LNV processes [4], which highlights the impact of $0\nu\beta\beta$ beyond neutrino physics.

For $0\nu\beta\beta$ with the exchange of the light Majorana neutrinos, the decay rate Γ is:

$$\Gamma = G^{0\nu}(Q)|M^{0\nu}|^2 \frac{|\langle m_{\beta\beta}\rangle|^2}{m_e^2}, \tag{1}$$

where , and $G^{0\nu}(Q)$ is phase space factor, $M^{0\nu}$ the nuclear matrix element, m_e the electron mass, and $|\langle m_{\beta\beta}\rangle|$ the effective Majorana neutrino mass. $G^{0\nu}(Q)$ is proportional to the 5th order of decay Q-value and can be accurately calculated [5]. Different model calculations of $M^{0\nu}$ may disagree by a factor of 2 to 3 and introduce large spread of $|\langle m_{\beta\beta}\rangle|$ [6, 7, 8, 9, 10, 11, 12]. The effective mass $|\langle m_{\beta\beta}\rangle|$ correlates $0\nu\beta\beta$ with neutrino mixing parameters closely: $|\langle m_{\beta\beta}\rangle| = \sum_{i=1}^{3} U_{ei}^2 m_i$, where U_{ei} are the elements in the first row of the neutrino mixing PMNS (Pontecorvo-Maki-Nakagawa-Sakata) matrix [13, 14] and m_i the three neutrino mass eigenvalues [1]. Current generation of $0\nu\beta\beta$ experiments, running or under construction, are generally sensitive to $m_{\beta\beta}$ in the range of 50 to 200 meV, while next generation experiments aim to cover the inverted hierarchy parameter space whose lower boundary is about 10 meV.

Experimentally, $0\nu\beta\beta$ experiments measure the energy of the two emitting electrons and search for a peak at the decay Q-value in the summed electron energy spectrum. Currently, more than 10 experiments worldwide aim to search for $0\nu\beta\beta$ utilizing techniques such as ionization, scintillation, thermal excitation, or some combination of those. For searches for $0\nu\beta\beta$ with half-lives longer than 10^{24} years, stringent requirements on parent isotope mass, detector energy resolution, and background rate are all critical. The commonly accepted figure of merit expression for the half-life limit of $0\nu\beta\beta$ is

$$T_{1/2}^{0\nu} \propto \eta \cdot a \cdot \sqrt{\frac{M \cdot t}{b \cdot \Delta E}}, \tag{2}$$
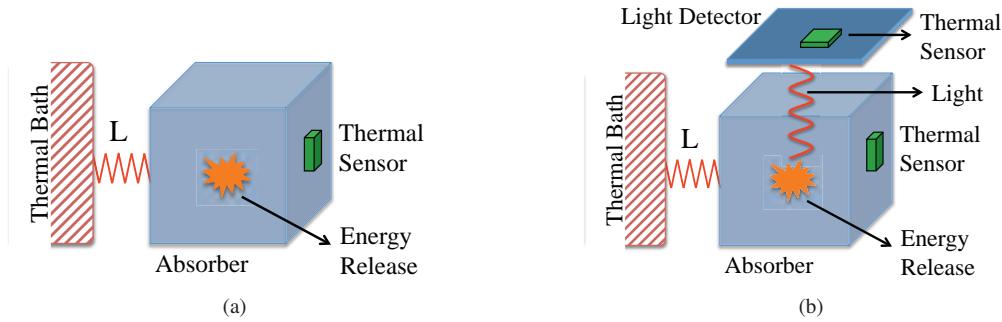
---
*email: cuore-spokesperson@lngs.infn.it
[1]Deceased

Fig. 1: (a) A schematic setup of typical bolometers. L is weak thermal link between the crystal and the thermal bath. (b) A similar schematic set for bolometers with an auxillary thin-slab bolometer on top to measure the light output. The light can come from either Cherenkov radiation or scintillation.

for background-limited case, where η is the physical detector efficiency, a the isotopic abundance of the $0\nu\beta\beta$ candidate, M the total detector mass, t the detector live time, b the background rate per unit detector mass per energy interval, and ΔE is the energy resolution of the detector [15]. For the background free (or signal-limited) searches, the half-life limit is proportional to the exposure $M \cdot t$:

$$T^{0\nu}_{1/2} \propto \eta \cdot a \cdot (M \cdot t). \tag{3}$$

The detector energy resolution ΔE does not appear in the equation above, but the "background-free" criteria impose strict requirement on energy resolution and background rejection of a specific experiment.

CUORE search for $0\nu\beta\beta$ of ^{130}Te using a large bolometer array of TeO$_2$ crystals. ^{130}Te is an attractive choice as $0\nu\beta\beta$ emitter for a couple of reasons. The natural isotopic abundance of ^{130}Te (34.2%) is highest among all the $0\nu\beta\beta$ candidate isotopes [16], and therefore no isotopic enrichment is necessary for CUORE. The decay Q-value is measured to be around 2528 keV [17, 18, 19], which is higher than most naturally occurring γ-ray background. The relatively high Q-value also means favorable phase space factor in Equation 1. The previous half-life limit of ^{130}Te was established by the CUORE predecessor experiment Cuoricino at 2.8×10^{24} y (90% C.L.) [20].

CUORE bolometer array features large detector mass and excellent energy resolution at region of interest (ROI). In this article, we review the advantages of bolometric technique in searching for $0\nu\beta\beta$ and give an update on latest CUORE progress. CUORE sensitivity will be limited by background, most of which are α particles from the surface of detector materials and nearby copper thermal shielding. Therefore, future generations of bolometer array, such as the Inverted Hierarchy Explorer (IHE) discussed in [21], focus on background suppression by detecting photon as well as the phonon signal. The photon signal comes either from Cherenkov radiation or scintillation of $0\nu\beta\beta$ emitting electrons. Section 4 discusses the physics and sensitivity in searching for $0\nu\beta\beta$ of ^{130}Te and other candidate isotopes at the IHE.

2. CUORE bolometric technique to search for $0\nu\beta\beta$

2.1. Bolometer design

A cryogenic bolometer measures energy release in an absorber via its temperature rise. As shown in Figure 1a, the temperature rise is usually picked up by a sensitive thermal sensor attached on the absorber. Because the extremely low phonon excitation energy at cryogenic temperature, the intrinsic sensitivity and resolution of bolometers are unparalleled to any other types of energy detection mechanism. For example, at 10 mK, the thermal phonon energy is about 1 peV, comparing to $\sim$ 3 eV of an electron-hole pair in semiconductors.

Bolometers for $0\nu\beta\beta$ searches have massive absorber to maximize the number of the candidate nuclei in it. To minimize the heat capacity of the absorber, dielectric crystals are usually the choice of absorber.

Thermal sensors are of many different types [22], the most widely used of which are resistive sensors (i.e. thermistors) such as Neutron Transmutation Doped (NTD) germanium thermistor and superconducting Transition Edge Sensor (TES). Microwave Kinetic Inductance Devices (MKIDs) and metallic magnetic sensors have gained popularity in recent years for low temperature detector application.

2.2. The CUORE experiment

The CUORE bolometer array will consist of 988 independent TeO_2 crystal modules arranged in 19 towers (Figure 2a). Each tower has 13 floors with 4 modules on each floor in a two by two configuration. The main component of each module is a 750 g, 5-cm cubic TeO_2 crystal grown from natural tellurium. The crystals were manufactured by the Shanghai Institute of Ceramics, Chinese Academy of Sciences with major input from the CUORE collaboration on quality and radio purity control [23]. The total detector mass is 741 kg and [130]Te isotope mass is 206 kg. The NTD Ge thermistor on each module is $3 \times 3 \times 1$ mm^3 and features good reproducibility, excellent stability and low noise. The thermistors follow nicely the Mott's law $R = R_0 \exp(\sqrt{T_0/T})$ [24], where $T_0 \sim 4$ K and $R \sim 1$ Ω. Besides the thermal sensor, each bolometer module is also instrumented with a Joule heater, which is used to inject a time-tagged, fixed amount of energy in the bolometer for offline thermal gain correction.

The Full Width Half Maximum (FWHM) resolution at ROI is expected to be 5 keV. Energy resolution of large-mass bolometers are dominated by thermal fluctuation from vibration and readout electronics. From CUORE-0 first phase data, we evaluate the overall detector energy resolution to be 5.7 keV, based on the FWHM of the 2615 keV peak in the energy spectrum for $0\nu\beta\beta$ searches [25, 26]. Recently, we have reduced the vibration from the CUORE-0 cryostat and saw noticeable improvement in the energy resolution. It should be also noted that CUORE-0 has been running at a base temperature range 13–15 mK, higher than expected CUORE base temperature at 10 mK. In our R&D runs, when the bolometers were operated below 13 mK, we consistently achieved energy resolution below 5 keV [27].

The projected background rate at ROI is 0.01 counts/keV/kg/y, which is mainly from surface and bulk contaminations of the bolometer components and the innermost copper thermal shield. Surface-related background, mainly α particles originated from the copper surface is 1–2×10^{-2} counts/keV/kg/y, based on Monte Carlo simulations with the latest results of CUORE-0 [28]. Background contribution from bulk contamination, predominately γ events from [208]Tl, is expected to be less than 6×10^{-3} counts/keV/kg/y (90% C.L.) [28].

CUORE will be situated at the LNGS underground facility at an average depth of 3650 m water equivalent, where the muon flux is $(2.58 \pm 0.3) \times 10^{-8}$ $\mu/(s \cdot cm^2)$, about six order of magnitude smaller than that of sea level [29]. The CUORE cryostat will be surrounded by borated polyethylene, boric-acid powder, and lead bricks to attenuate neutron and γ-ray backgrounds. More lead shielding is added inside the cryostat, including ancient Roman lead [30] to further suppress the γ-rays. We find the expected environmental muon, neutron, and γ background rates in the ROI to be orders of magnitude smaller than the α and γ backgrounds from the experimental apparatus itself [31, 32].

CUORE sensitivity is limited by the background and follows Equation 2. A more rigorous sensitivity projection based on Poissonian background fluctuation shows that CUORE projected half-life sensitivity is 1.6×10^{26} y at 1σ (9.5×10^{25} y at the 90% C.L.) [15], which corresponds to an upper limit on the effective Majorana mass in the range 40 –100 meV (50 –130 meV). The lower and upper bound of $m_{\beta\beta}$ is calculated with the most and least favorable NME [6, 7, 8, 9, 10, 11, 12].

2.3. Additional advantage of bolometer for $0\nu\beta\beta$ search

Typically we categorize searches for $0\nu\beta\beta$ into two groups by the relation of $0\nu\beta\beta$ source and detector. One common approach is to implement a detector with candidate isotope inside. For example, GERDA uses semiconductor [76]Ge-enriched germanium diode to search for $0\nu\beta\beta$ of [76]Ge [33]. The "source in detector" approach has the advantage of high detecting efficiency. The other approach emphasizes on the flexibility of $0\nu\beta\beta$ source choices by separating the source from detection, the typical example of which is the NEMO3/SuperNEMO project [34].

Bolometric technique combines the benefits of high efficiency and flexibility of candidate isotope choice. For large-mass bolometers such as CUORE modules, the probability of both $0\nu\beta\beta$ electrons are confined
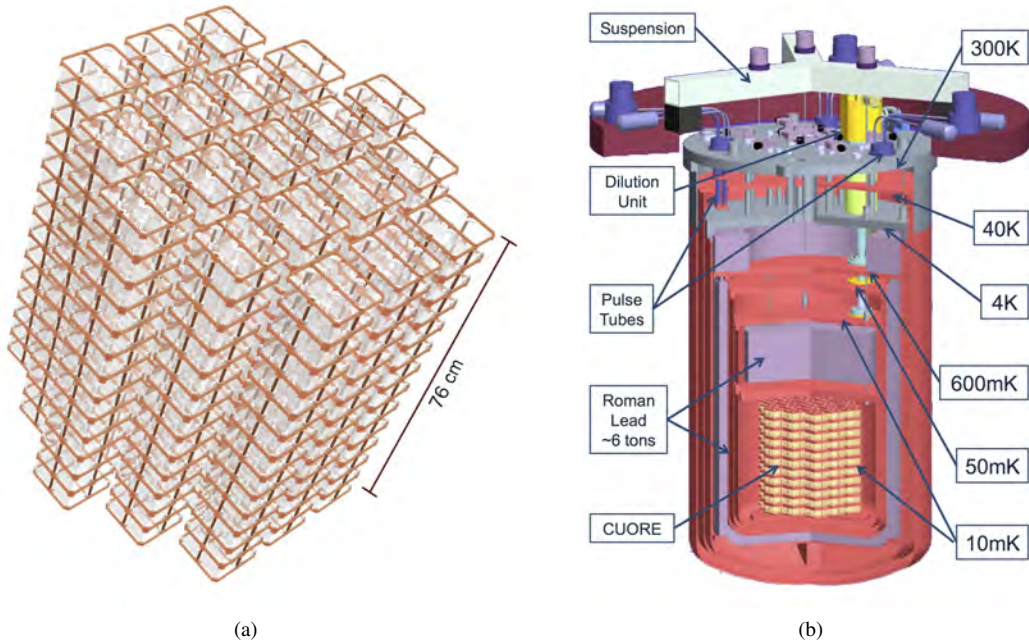
(a)   (b)

Fig. 2: (a) Schematic setup of CUORE towers. 19 towers are closely packed. Each tower has 13 floors and 4 bolometer modules on each floor. (9) CUORE cryostat with major components highlighted.

in the crystal is $(87.4 \pm 1.1)\%$. Bolometric technique puts little constraints on the absorber materials, other than preferably dielectric for the benefit of small heat capacity. Crystals such as TeO_2 or ZnSe are easily interchangeable for search of $0\nu\beta\beta$ in different candidate isotopes. The flexibility is especially useful for confirming $0\nu\beta\beta$ discoveries or cross-comparing $m_{\beta\beta}$ limits in different isotopes.

3. CUORE status

Ongoing CUORE construction includes major effort on bolometer array assembly, cryostat commissioning, detector calibration system (DCS) integration, electronics and software development.

3.1. Detector assembly

During the bolometer array assembly process, we need to turn 10000 loose parts into 988 ultra-clean bolometer modules. All the operations are conducted in glove boxes under nitrogen atmosphere to minimize oxidization and contamination of radon and radon progenies [35]. The assembly process starts by gluing of thermistors and heaters to crystals with a robotic system to maintain the uniformity and repeatability of the gluing joints. Then we assemble the instrumented crystals, cleaned copper parts, and PTFE spacers into a tower. Along the two wire trays on opposite side of each tower, we attach two sets of flexible printed circuit board readout cables, whose top ends will be connected to the cryostat wiring later. The bottom ends of the readout cables are terminated with copper bonding pads. In the final step of detector assembly, we use a wire bonder to bond the thermistors and heaters to the bonding pads to complete the electrical connections.

CUORE tower assembly began in January 2013 and will be finished by summer of 2014. As of this writing we have glued 15 tower's worth of crystals, physically assembled 13 towers, and wire bonded 12. More details on CUORE detector assembly can be found in [27].
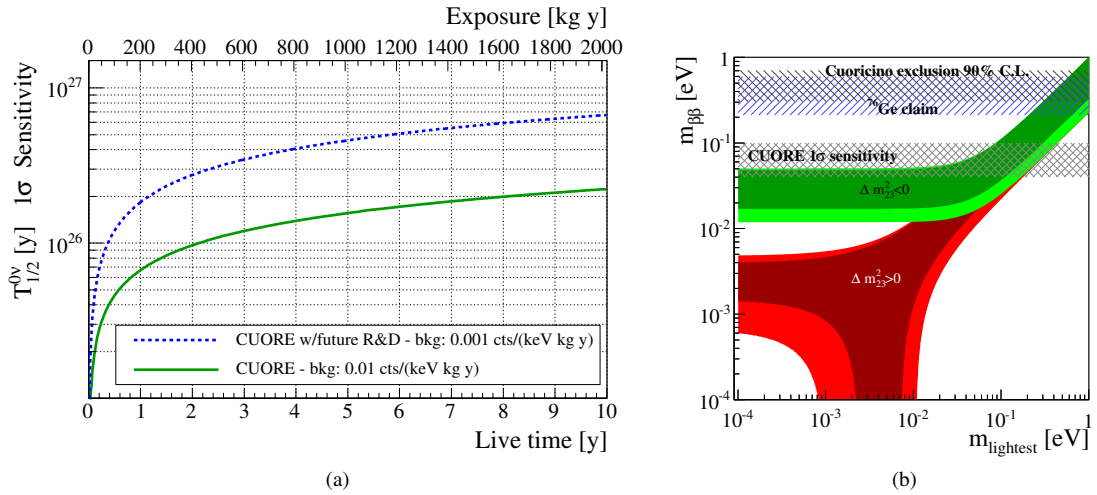
Fig. 3: (a) Projected CUORE 1σ sensitivity to the half-life of $0\nu\beta\beta$ of ^{130}Te as a function of detector live time. The solid green line shows the sensitivity for the target background rate of 0.01 counts/keV/kg/y, while the dashed blue line shows an optimistic scenario of 0.001 counts/keV/kg/y background rate. (b) The corresponding 1σ sensitivity to effective Majorana mass versus lightest neutrino mass after five years of detector live time. The spread in the projected CUORE $m_{\beta\beta}$ bands arises from uncertainties in calculations of the nuclear matrix elements used to convert a measured half-life into an effective Majorana mass. The green band labeled $\Delta m_{23}^2 < 0$ denotes the inverted neutrino mass hierarchy while the red band labeled $\Delta m_{23}^2 > 0$ indicates the normal mass hierarchy. For both, the darker inner bands represent regions allowed by the best-fit neutrino oscillation parameters in the PMNS matrix, while the lighter outer bands extend to 3σ coverage. Both figures are from [15].

3.2. Cryogenics

CUORE cryogenics system cools the bolometer array and the immediate shielding, almost 7 ton of material, to 10 mK base temperature. The system includes a large cryostat with six nested thermal shields, a cryogen-free cooling system with five pulse-tube coolers, an auxiliary fast-cooling system for pre-cooling, and a dilution-refrigerator unit [36].

All six copper thermal shields of the cryostat have been delivered to LNGS underground facility for commissioning. In the first phase of cryostat commissioning, we cooled down the outer three vessels with three pulse tubes twice, successfully reaching 3.5 K on the 4 K plate on the second attempt [37]. The second phase of commissioning with three inner vessels is currently ongoing. In addition to the pulse tubes and closed-loop pre-cooling circulation lines, an auxiliary fast-cooling system circulates helium gas through the cryostat vessels to speed up the cooling from room temperature to 4 K.

The custom-built ^{3}He/^{4}He dilution unit by Leiden Cryogenics was delivered in Summer 2012 after passing in-house benchmarking. At LNGS it was tested in a small testing cryostat and successfully reached 5 mK base temperature with a cooling power of 5 μW at 12 mK. The unit will be integrated to the main cryostat after the commissioning of the inner thermal shields.

3.3. Detector Calibration System

DCS is designed to insert and retrieve 12 radioactive source strings from the 300 K top flange to the bolometer array at 10 mK for energy calibrations every month. The main challenge is to limit the heat-load while lowering the source strings through the successive flanges with decreasing temperatures. Along each Kevlar string, we crimp 25 thoriated tungsten sources, evenly separated by 29 mm from each other. A motion control system on top of the 300 K flange releases each string to travel down a dedicated guide tube by its own weight. The strings are thermalized at the 4 K flange to avoid over-heating the three inner cryostat

Isotope	Q-Value [keV]	Crystal	Exposure [ton·y]	Background [counts/ton/y]	$\|m_{\beta\beta}\|_{discovery}$ [meV]	$\widehat{T^{0\nu}_{1/2}}$ $[10^{27}\text{y}]$	$\|m_{\beta\beta}\|_S$ [meV]
^{82}Se	2996	ZnSe	3.3	0.1	18 - 52	2.2	11 - 32
^{116}Cd	2814	$CdWO_4$	4.9	0.1	24 - 45	1.5	14 - 26
^{100}Mo	3034	$ZnMoO_4$	2.7	1.5	24 - 69	0.65	13 - 37
^{130}Te	2528	TeO_2	3.7	0.1	17 - 43	2.6	10 - 25

Table 1: Four candidate isotopes considered for the IHE. The exposure assumes five year live time. Background rates are assumed to be 0.1 counts/ton/y except for the ^{100}Mo case, which is higher because of $2\nu\beta\beta$ events pile-up. Assuming neutrinos are of Majorana type, IHE would discover a signal of 5σ or larger if the effective Majorana mass is at least $\|m_{\beta\beta}\|_{discovery}$. $\widehat{T^{0\nu}_{1/2}}$ and $\|m_{\beta\beta}\|_S$ are 90% C.L. sensitivity to $0\nu\beta\beta$ half-life and effective Majorana mass. The range of $\|m_{\beta\beta}\|$ reflects the uncertainties of different model calculations of NME. Data from [21].

vessels. DCS was successfully tested to the 4 K flange together with a commissioning cooldown of the outer cryostat as mentioned earlier. We will further test the DCS along with future cryostat commissioning cool downs.

3.4. Electronics, data acquisition, and analysis

The CUORE electronics will read the thermistor voltage signal to computer via the front end electronics, high-precision 18-bit digitizers, and the data acquisition software APOLLO. Each front-end channel consists of load resistors, a detector biasing system, a two-stage amplifier system with programmable gain up to 10000, and a 6-pole anti-aliasing Bessel filter with cutoff frequencies in the range 15–120 Hz. We have prepared a single chassis system with a full chain CUORE electronics for testing on a mini bolometer array during upcoming commissioning tests of the CUORE cryostat.

The DAQ software APOLLO reads in the digitized waveforms at 125 S/s, runs trigger algorithms, and records both the continuous and triggered data on the disk for offline analysis. APOLLO has been used successfully for CUORE-0 data taking [25]. Current development focuses on scaling from one DAQ computer use case (as in CUORE-0) to a small DAQ cluster to acquire the ~1000 channels in CUORE. Our custom-built data analysis software framework DIANA has been used extensively for analysis of Cuoricino, R&D runs, and more recently CUORE-0. New features such as noise decorrelation [38] and browser-based data quality monitoring are being implemented.

4. Inverted Hierarchy Explorer – bolometer with light output

Background suppression with particle identification is the main emphasis on bolometer's future application in rare event searches. Additional detection channels are needed for particle identification since the absorber does not respond differently for energy release of different particle types. To distinguish between $0\nu\beta\beta$ electrons and α particle background, light emission, either from Cherenkov radiation or scintillation, can be exploited. The auxiliary light detector is usually another bolometer facing the main bolometer. The light detector nominally consists of a thin germanium/silicon wafer as absorber and a thermal sensor of the same type as the main bolometer.

The next generation bolometric experiment with light output, which we call Inverted Hierarchy Explorer (IHE), aims to explore the inverted neutrino mass hierarchy region at effective Majorana mass $m_{\beta\beta} \sim$ 10 meV [21]. We have studied the sensitivities of TeO_2 bolometers with Cherenkov light readout and three scintillating bolometers ZnSe, $CdWO_4$, and $ZnMoO_4$, all of which are hosted in a dilution refrigerator similar to CUORE (see Figure 2b).

The TeO_2 crystal is largely transparent to Cherenkov light radiation generated by electrons with energy larger than 50 keV [39]. Should the Cherenkov light from electrons observable, it provides a definite discrimination between α backgrounds and electrons. For typical bolometer α background, their energy is an

order of magnitude lower than the Cherenkov radiation threshold in TeO_2. Cherenkov light emission in TeO_2 has been detected using a secondary light detector with modest particle identification capability [40]. We are actively developing better light collection schemes and more importantly, light detectors with lower threshold and better energy resolution. Future directions include new thermal sensors on the light detector, such as TES [41] and MKIDs [42], and Luke effect [43] enhanced bolometers.

A scintillating bolometer operates similarly to the Cherenkov case, but with a different crystals and more light output from scintillation. The particle identification comes from the different light yield for different particle type. For scintillating crystals such as ZnSe, $CdWO_4$, and $ZnMoO_4$, the light yield difference between possible $0\nu\beta\beta$ electrons and α particles are well measured [44, 45, 46, 47, 48, 49, 50, 51].

IHE detector will consist of 988 bolometer modules, each with a 5-cm cubic crystal of our choice. The detector arrangement follows CUORE design. The four bolometer modules on each floor shares a light detector made of radio-pure germanium or silicon wafer of about 300 μm thick and 10 cm in diameter. The crystals are wrapped in reflecting foils to improve the light collection efficiency. The natural isotopic abundance of ^{82}Se, ^{116}Cd and ^{100}Mo are all less than 10%. In IHE, we assume all $0\nu\beta\beta$ candidate isotopes are enriched to 90%.

The physics reach of IHE for the different $0\nu\beta\beta$ candidate isotopes are reported in Table 1 with 5 years of live time and ΔE= 5 keV. In the table, we make aggressive assumption on background reduction and an optimistic background index of 0.1 counts/ton/y (1.5 counts/ton/y for the $ZnMoO_4$ case due to the pile-up of the intrinsic $2\nu\beta\beta$ events) is assumed. More information about the background budget and effectiveness of background suppression can be found in [21]. In the last three columns of the table, we present the minimum observable value of the effective Majorana mass $|m_{\beta\beta}|_{discovery}$ for a $0\nu\beta\beta$ discovery and 90% C.L. sensitivity on half-life and $|m_{\beta\beta}|_S$ for a null result. Assuming neutrinos are of Majorana type, IHE would discover a signal of 5σ or larger if the effective Majorana mass is at least $|m_{\beta\beta}|_{discovery}$. The 90% C.L. half-life sensitivities are all on the 10^{27} y level. The TeO_2 case is especially sensitive to the effective Majorana mass at 10 to 25 meV, reaching the lower boundary of the inverted mass hierarchy.

5. Conclusion and outlook

We reviewed the physics reach and current construction status of the CUORE experiment. Data taking is expected to start in 2015. With excellent energy resolution and large isotope mass, CUORE is one of the most competitive $0\nu\beta\beta$ experiments under construction.

Future bolometer program such as the IHE can explore the inverted mass hierarchy region to $|m_{\beta\beta}| \sim$ 10 meV by utilizing additional light readout to further reduce background. We described the conceptual design of IHE and its physics impact on ^{130}Te, ^{82}Se, ^{116}Cd or ^{100}Mo $0\nu\beta\beta$ searches.

References

[1] J. Beringer, et al., The review of particle physics, Phys. Rev. D86 (2012) 010001.
[2] F. T. Avignone, S. R. Elliott, J. Engel, Double beta decay, Majorana neutrinos, and neutrino mass, Rev. Mod. Phys. 80 (2) (2008) 481–516.
[3] S. M. Bilenky, C. Giunti, Neutrinoless double-beta decay. a brief review, arXiv:1203.5250.

[4]   A. de Gouvea, P. Vogel, Lepton flavor and number conservation, and physics beyond the standard model, arXiv:1303.4097.
[5]   J. Kotila, F. Iachello, Phase-space factors for double- decay, Physical Review C 85 (3) (2012) 034316.
[6]   J. Menendez, A. Poves, E. Caurier, F. Nowacki, Disassembling the Nuclear Matrix Elements of the Neutrinoless beta beta Decay, Nucl. Phys. A 818 (2009) 139–151. `arXiv:0801.3760,`
[7]   P. K. Rath, et al., Uncertainties in nuclear transition matrix elements for $\beta + \beta+$ and $\epsilon\beta+$ modes of neutrinoless positron double-β decay within the projected hartree-fock-bogoliubov model, Phys. Rev. C 87 (2013) 014301.
[8]   T. R. Rodriguez, G. Martinez-Pinedo, Energy density functional study of nuclear matrix elements for neutrinoless $\beta\beta$ decay, Phys. Rev. Lett. 105 (2010) 252503. `arXiv:1008.5260,`
[9]   D.-L. Fang, A. Faessler, V. Rodin, F. Simkovic, Neutrinoless double beta decay of deformed nuclei within QRPA with realistic interaction, Phys. Rev. C 83 (2011) 034320. `arXiv:1101.2149,`
[10] A. Faessler, V. Rodin, F. Simkovic, Nuclear matrix elements for neutrinoless double-beta decay and double-electron capture, J. Phys. G: Nucl. Part. Phys. 39 (2012) 124006. `arXiv:1206.0464,`
[11] J. Suhonen, O. Civitarese, Review of the properties of the $0\nu\beta\beta$ nuclear matrix elements, J. Phys. G: Nucl. Part. Phys. 39 (12) (2012) 124005.
[12] J. Barea, J. Kotila, F. Iachello, Nuclear matrix elements for double-β decay, Phys. Rev. C 87 (2013) 014315. `arXiv:1301.4203,`
[13] B. M. Pontecorvo, Mesonium and antimesonium, J. Exp. Theor. Phys. Lett. 33 (1957) 549.
[14] Z. Maki, M. Nakagawa, S. Sakata, Remarks on the unified model of elementary particles, Prog. Theor. Phys. 28 (5) (1962) 870–880.
[15] F. Alessandria, et al., Sensitivity of CUORE to neutrinoless double-beta decay, arXiv:1109.0494.
[16] M. A. Fehr, M. Rehkamper, A. N. Halliday, Application of MC-ICPMS to the precise determination of tellurium isotope compositions in chondrites, iron meteorites and sulfides, Int. J. Mass spectrom. 232 (2004) 83–94.
[17] M. Redshaw, B. J. Mount, E. G. Myers, F. T. Avignone, III, Masses of ^{130}Te and ^{130}Xe and double-β-decay Q-value of ^{130}Te, Phys. Rev. Lett. 102 (21) (2009) 212502. `arXiv:0902.2139.`
[18] N. D. Scielzo, et al., Double-β-decay Q values of ^{130}Te, ^{128}Te, and ^{120}Te, Phys. Rev. C80 (2009) 025501. `arXiv:0902.2376.`
[19] S. Rahaman, et al., Double-beta decay Q values of 116Cd and 130Te, Phys. Lett. B 703 (4) (2011) 412.
[20] E. Andreotti, et al., 130Te Neutrinoless Double-Beta Decay with CUORICINO, Astropart. Phys. 34 (2011) 822–831. `arXiv:1012.3266.`
[21] D. R. Artusa, et al., The frontier of neutrinoless double beta decay with bolometers, to be submitted (2014).
[22] C. Enss (Ed.), Cryogenic Particle Detection, Springer-Verlag Berlin Heidelberg, 2005.
[23] C. Arnaboldi, et al., Production of high purity TeO$_2$ single crystals for the study of neutrinoless double beta decay, J. Cryst. Growth 312 (20) (2010) 2999–3008. `arXiv:1005.3686.`
[24] D. McCammon, Semiconductor thermistors, Appl. Phys. 99 (2005) 35–61. `arXiv:physics/0503086.`
[25] D. R. Artusa, et al., Initial performance of the CUORE-0 experiment, arXiv:1402.0922.
[26] D. R. Artusa, et al., First data of CUORE-0, this proceedings.
[27] D. R. Artusa, et al., Searching for neutrinoless double-beta decay of ^{130}Te with CUORE, arXiv:1402.6072.
[28] D. R. Artusa, et al., Projected background budget of the CUORE experiment, to be submitted.
[29] D. Mei, A. Hime, Muon-Induced Background Study for Underground Laboratories, Phys. Rev. D73 (2006) 053004. `arXiv:astro-ph/0512125,`
[30] A. Alessandrello, et al., Measurements of internal radioactive contamination in samples of Roman lead to be used in experiments on rare events, Nucl. Instrum. Meth. B142 (1998) 163.
[31] E. Andreotti, et al., Muon-induced backgrounds in the CUORICINO experiment, Astropart. Phys. 34 (2010) 18–24. `arXiv:0912.3779,`
[32] F. Bellini, et al., Monte carlo evaluation of the external gamma, neutron and muon induced background sources in the CUORE experiment, Astropart. Phys. 33 (2010) 169.
[33] M. Agostini, et al., Results on neutrinoless double beta decay of 76Ge from GERDA Phase I, Phys. Rev. Lett. 111 (2013) 122503. `arXiv:1307.4720,`
[34] A. S. Barabash, SuperNEMO double beta decay experiment, arXiv:1112.1784.
[35] M. Clemenza, C. Maiano, L. Pattavina, E. Previtali, Radon-induced surface contaminations in low background experiments, Eur. Phys. J. C71 (2011) 1805.
[36] A. Nucciotti, et al., Status of the Cryogen-Free Cryogenic System for the CUORE Experiment, Journal of Low Temperature Physics 167 (2012) 528–534.
[37] E. Ferri, et al., Commissioning of the 4 K Outer Cryostat for the CUORE Experiment, Journal of Low Temperature Physics (2014) 1–7.
[38] C. Mancini-Terracciano, M. Vignati, Noise correlation and decorrelation in arrays of bolometric detectors, JINST 7 (2012) P06013. `arXiv:1203.1782.`
[39] T. Tabarelli de Fatis, Cherenkov emission as a positive tag of double beta decays in bolometric experiments, Eur. Phys. J. C65 (2010) 359.
[40] J. Beeman, et al., Discrimination of alpha and beta/gamma interactions in a TeO$_2$ bolometer, Astropart. Phys. 35 (2012) 558. `arXiv:1106.6286,`
[41] G. Angloher, et al., Results from 730 kg days of the CRESST-II Dark Matter Search, Eur. Phys. J. C72 (2012) 1971. `arXiv:1109.0702,`
[42] S. Domizio, et al., Cryogenic wide-area light detectors for neutrino and dark matter searches, J. Low. Temp. Phys. (2014) 1–7
[43] C. Isaila, et al., Low-temperature light detectors: Neganov-Luke amplification and calibration, Phys. Lett. B 716 (1) (2012) 160.
[44] S. Pirro, et al., Scintillating double-beta-decay bolometers, Phys. Atom. Nucl. 69 (2006) 2109.
[45] C. Arnaboldi, et al., Characterization of ZnSe scintillating bolometers for Double Beta Decay, Astropart. Phys. 34 (2011) 344.

arXiv:1006.2721,

[46] J. W. Beeman, et al., Performances of a large mass ZnSe bolometer to search for rare events, Journal of Instrumentation 8 (2013) 05021.

[47] C. Arnaboldi, et al., CdWO$_4$ scintillating bolometer for Double Beta Decay: Light and Heat anticorrelation, light yield and quenching factors, Astropart. Phys. 34 (2010) 143. arXiv:1005.1239,

[48] J. Beeman, et al., A next-generation neutrinoless double beta decay experiment based on ZnMoO$_4$ scintillating bolometers, Phys. Lett. B 710 (2) (2012) 318.

[49] L. Gironi, et al., Performance of ZnMoO$_4$ crystal as cryogenic scintillating bolometer to search for double beta decay of molybdenum, JINST 5 (2010) P11007. arXiv:1010.0103,

[50] J. Beeman, et al., ZnMoO4: A promising bolometer for neutrinoless double beta decay searches, Astropart. Phys. 35 (12) (2012) 813.

[51] J. Beeman, et al., Performances of a large mass ZnMoO$_4$ scintillating bolometer for a next generation neutrinoless double beta decay experiment, Eur. Phys. J. C72 (2012) 1.